HHS Public Access

Author manuscript

J Leukoc Biol. Author manuscript; available in PMC 2019 July 29.

Structural insights into Resolvin D4 actions and further metabolites *via* a new total organic synthesis and validation

Jeremy W. Winkler[*], **Stephania Libreros**[*], **Xavier De La Rosa**[*], **Brian E. Sansbury**[*], **Paul C. Norris**[*], **Nan Chiang**[*], **David Fichtner**[†], **Gregory S. Keyes**[†], **Nicholas Wourms**[†], **Matthew Spite**[*], and **Charles N. Serhan**[*,1]

[*]Center for Experimental Therapeutics and Reperfusion Injury, Department of Anesthesiology, Perioperative and Pain Medicine, Building for Transformative Medicine, Brigham and Women's Hospital and Harvard Medical School, Boston, Massachusetts 02115 U.S.A.

[†] Cayman Chemical, Ann Arbor, MI 48108, USA

Abstract

Local production and downstream metabolism of specialized pro-resolving lipid mediators (SPMs) are pivotal in regulating their biological actions during resolution of inflammation. Resolvin D4 (RvD4 – 4*S*,5*R*,17*S*-trihydroxydocosa-6*E*,8*E*,10*Z*,13*Z*,15*E*,19*Z* hexaenoic acid) is one of the more recently elucidated SPMs with complete stereochemistry biosynthesized from docosahexaenoic acid (DHA). Here, we report a new multi-milligram commercial synthesis that afforded enough material for matching, validation and further evaluation of RvD4-functions. Using LC-MS-MS profiling, RvD4 was identified at bioactive amounts in human (1 pg/ml) and mouse bone marrow (12 pg/femur and tibia). In mouse bone marrow, ischemia increased the formation of RvD4 >37-fold (455 pg/femur and tibia). Two separate mouse ischemic injury models were used, where RvD4 reduced second organ reperfusion lung injury >50%, demonstrating organ-protection. Structure-function relationships of RvD4 demonstrated >40% increase in neutrophil and monocyte phagocytic function in human whole blood in comparison with two separate trans-containing double-bond isomers that were inactive. These two isomers were prepared by organic synthesis: 4*S*,5*R*,17*S*-trihydroxydocosa-6*E*,8*E*,10*E*,13*Z*,15*E*,19*Z*-hexaenoic acid (10-trans-RvD4), a natural isomer, and 4*S*,5*R*,17*S*-trihydroxydocosa-6*E*,8*E*,10*E*,13*E*,15*E*,19*Z*-hexaenoic acid (10,13-trans-RvD4), a double isomer. Compared to leukotriene B_4, D-series resolvins (RvD1, RvD2, RvD3, RvD4, or RvD5) did not stimulate human neutrophil chemotaxis monitored via real-time microfluidics chambers. A novel 17-oxo-containing-RvD4 product of eicosanoid oxidoreductase (EOR) was identified with human bone marrow cells. Comparison of 17-oxo-RvD4 to RvD4 demonstrated that with human leukocytes 17-oxo-RvD4 was inactive. Together, these provide commercial-scale synthesis that permitted a second independent validation of RvD4 complete

[1]Corresponding author: Prof. Charles N. Serhan, Center for Experimental Therapeutics and Reperfusion Injury, Building for Transformative Medicine, 60 Fenwood Rd. #3016, Boston, MA 02115, USA. cserhan@bwh.harvard.edu.

Authorship

C.N.S. conceived of the studies and contributed to manuscript preparation. J.W.W., S.L., X.D.L.R., B.E.S., P.C.N. and N.C. carried out matching and bioactions of RvD4, related isomers and metabolites. G.S.K., D.F. and N.W. carried out total organic synthesis. All authors contributed to manuscript preparation and writing of the manuscript.

Conflict of Interest Disclosure

The authors declare no conflict of interest.

stereochemical structure as well as evidence for RvD4 regulation in tissues and its stereoselective phagocyte responses.

Summary sentence:

Resolvin D4 commercial-scale total organic synthesis elucidates new functions.

Keywords

Ischemia; reperfusion injury; anti-inflammatory; specialized pro-resolving mediators; resolvins; oxidoreductase; essential fatty acids; leukocytes

Introduction

Several new families of lipid mediators derived from polyunsaturated fatty acids (PUFA) termed specialized pro-resolving mediators (SPMs) have recently been described for their importance in signaling endogenous programs in the resolution of inflammation and clearance of infection [1]. D-series resolvins are a subset of SPMs derived from docosahexaenoic acid (DHA) that have potent anti-inflammatory and pro-resolving actions [1, 2]. The acute inflammatory response is host protective, ideally self-limited, and follows an elaborate orchestration of neutrophilic recruitment to the site of injury, and its resolution, which involves cessation of neutrophil influx and macrophage-mediated clearance of cellular debris and bacteria [3, 4]. Resolvins are agonists acting at picomolar to nanomolar potency to dampen as well as counter-regulate the initiators of this response (such as prostaglandins, cytokines and chemokines) allowing for recovery with shortened resolution intervals to terminate the acute response [1, 4]. The importance of understanding and improving therapies to target endogenous resolution programs of inflammation is of interest for preventative care as well as treatment of chronic inflammation that can lead to a variety of serious illnesses and pathologies [5, 6]. Importantly, agonists acting on these new resolution pathways could potentially resolve inflammation without common unwanted side effects associated with non-steroidal anti-inflammatory therapeutics (NSAIDs) [7, 8].

The essential role of pro-resolving mediators such as the D-series resolvins in infection and inflammation is further supported by the local mobilization of their precursor, DHA, at the site of injury during the cellular response to organ protection and repair [9–11]. During the acute inflammatory response, SPMs demonstrate several unique temporal and spatial profiles, being produced subsequent to the classical eicosanoids (i.e., prostaglandins and leukotrienes) that trigger pro-inflammatory cytokines and leukocyte recruitment [12]. Resolvins possess both anti-inflammatory and pro-resolving functions [1] based on their endogenous levels and release profile in response to tissue activation and damage [5, 13]. Downstream further metabolism can regulate the local function of resolvins during inflammation and infection [14, 15].

The local inflammatory response during ischemia is an area of interest as it is directly related to the acute and chronic inflammatory response observed following surgery (e.g., amputations or arterial bypass) [16]. A better understanding of the acute inflammation that

follows surgery and local ischemia is critical for developing more effective treatment strategies. For example, as physiologic stop signals for neutrophil influx, resolvins, such as RvD2, dampen pro-inflammatory responses, protecting organs from leukocyte-mediated collateral tissue damage and also by promoting tissue repair [17, 18]. Hind limb ischemia and reperfusion injury in mice are useful models of patients with arterial diseases [19] and second organ reflow injuries [19, 20]. Local production of potent SPMs at the site of injury is key for their broad-acting roles and unique actions on human leukocyte trafficking during the initiation and resolution of acute inflammation in mice [21].

The D-series resolvin substrate, DHA is enriched in the brain post cerebral ischemia during the inflammatory response and accumulates in the ischemic area post-surgical survival [22]. The biosynthesis of D-series resolvins involves metabolic conversion of DHA to monohydroperoxy precursors which then undergo enzymatic conversion into specific resolvins [23]. Resolvin D4 was first identified in self-limited mouse exudates and human leukocytes [23], and its complete stereochemistry was recently established [24]. RvD4 is present in skin infections and, upon completion of the first total synthesis, was found to play an active role in host protection during bacterial pathogenesis in the skin [24].

As with all endogenous chemical mediators, it is critical to validate and confirm the structures and actions of new pro-resolving mediators using materials prepared by total organic synthesis. Progress on the actions of resolvins is hampered by the cost of long and complex synthetic routes. Hence, in this report we describe a completely new total organic synthesis for larger-scale commercial production of RvD4, that also permitted further confirmation and validation of the RvD4 complete stereochemical structure as well as its potent stereoselective functions. We used two separate *in vivo* mouse models of ischemic injury to assess RvD4, i.e. ischemic bone [19] and second organ reperfusion (*e.g.* reflow) injury of the lung [20]. The biosynthesis of RvD4 was significantly increased in ischemic bone marrow and also proved to be organ protective in the reperfusion injury model. To explore the structure-function relationships and potential further local metabolism of RvD4, we also report herein the activity of RvD4 with direct comparison to other D-series resolvins (RvD1 to RvD5) and related RvD4 geometric isomers. Moreover, we report herein that RvD4 is enzymatically converted to a new 17-oxo-RvD4 metabolite, which displayed diminished bioactions compared to RvD4.

Materials and Methods

Chemical confirmation of Synthetic RvD4 and isomers

The proton chemical shift and coupling constants for the prepared RvD4 were recorded as follows (see Supplementary for further details). **(29):** ^{1}H NMR (400 MHz, CD_3OD, δ): 0.96 (t, J=7.6 Hz, 3H), 1.55–1.68 (m, 1H), 1.79–1.90 (m, 1H), 2.06 (q, J=7.5Hz, 2H), 2.21–2.52 (m, 4H), 3.11 (t, J=7.7Hz, 2H), 3.45–3.52 (m, 1H), 3.97 (t, J=6.3 Hz, 1H), 4.14 (q, J=6.2 Hz, 1H), 5.32–5.53 (m, 4H), 5.64–5.81 (m, 3H), 6.00 (t, J=10.8Hz, 1H), 6.05 (t, J=11.1Hz, 1H), 6.25 (dd, J=10.8, 14.6Hz, 1H), 6.39 (dd, J=10.8, 15.0Hz, 1H), 6.52–6.64 (m, 2H); UV (MeOH) λ_{max} 266, 276, 285 nm and λ_{max} shoulder of 233 nm; HPLC: Gemini C18, 5mm, 250 × 4.6 mm, monitored at 270 nm, MeOH/H_2O (0.1% AcOH) 75/25, 1 ml/min, T_R = 13.06 min. Synthetic isomers (see Supplementary Data for synthesis conditions) were

monitored by HPLC and UV-Vis on a Gemini C18, 5mm, 250 × 4.6 mm, monitored at 270 nm, MeOH/H_2O (0.1% AcOH) 70/30, 1 ml/min, T_R = 16.78 min for 10*E*-RvD4, 17.67 min for 10*E*,13*E*-RvD4, and 18.45 min for RvD4.

Models of ischemic injury:

a) Second organ ischemia reperfusion injury of the lung—Two separate models of ischemic tissue injury were used in the present evaluations of RvD4. All experimental procedures were approved by the Standing Committee on Animals of Brigham and Women's Hospital (protocol no. 2016N000145) and complied with institutional and US National Institutes of Health guidelines. For second organ injury, bilateral hind limb ischemia was initiated using tourniquets placed on each limb of 6–8-week-old male C57BL/6j mice [25]. Mice were subjected to ischemia for 1 hour, tourniquets were removed and reperfusion ensued for 2h. Ten min prior to tourniquet release (initiating reperfusion), vehicle (saline containing 0.1% ethanol) [20], RvD4 (500 ng/mouse) or RvD3 (500 ng/mouse) were administered i.v. Next, mice were euthanized and lungs collected for quantification of PMN infiltration and for LC-MS-MS metabolo-lipidomics (*vide infra*). Neutrophilic infiltration was quantified with a 1:10 cell-free supernatant of homogenate lungs by MPO ELISA as in [25].

b) Surgical induction of hind limb ischemia (HLI)—The surgical hind limb ischemia protocol was performed as in [17]. Briefly, the second ischemia model employed C57BL/6J mice that were anesthetized with 2% isoflurane (with 2 L/min O_2) and maintained on a temperature-controlled water blanket at 37°C (protocol no. 2016N000131). Hair was removed from the limb with depilatory cream followed by successive betadine and 70% ethanol washes in order to sterilize the incision area. A small incision was made lateral to the abdomen and superficial to the inguinal ligament exposing the inguinal fat pad. The overlying adipose tissue was set aside from the peritoneal lining and a small tissue retractor was inserted to reveal the proximal femoral artery at its branching from the internal iliac artery. The membrane sheath surrounding the femoral artery and vein was then removed and using ring forceps, both vessels were gently grasped and raised so that two ligatures could be passed underneath them. The ligatures were then positioned roughly 2 mm apart and tightened to occlude blood flow. Both vessels were transected between the ligatures, the adipose tissue was repositioned and the incision was closed with n-butyl-ester cyanoacrylate.

For sham-operated mice, an incision was made, the tissue was dissected to expose the vessels and ligatures were passed under the vessels but not tied and no flow was occluded. Buprenorphine (0.5 mg/kg) was given immediately prior to surgery and again within 24 hours post-surgery. Mice were euthanatized and marrow from the femur and tibia of each ischemic limb were flushed with 1 mL cold methanol before solid phase extraction with internal standards (*vide infra)* and targeted LC-MS-MS.

LM-SPM metabololipidomics

Liquid chromatography–tandem mass spectrometry-based metabololipidomics was performed with lungs or bone marrow cells from ischemic mice, as well as human bone marrow tissue purchased from the Cooperative Human Tissue Network at the University of

Pennsylvania (Philadelphia, PA, USA). Prior to sample extraction, two volumes of ice-cold methanol (EMD Millipore, MA USA) containing deuterium-labeled d_4-LTB_4, d_4-5S-HETE, d_4-PGE_2, and d_5-RvD2 internal standards (500 pg each) were added to each sample for purposes of quantification and recovery. All samples were kept at −20°C for 45 min to allow for protein precipitation, followed by centrifugation and then subjected to solid-phase extraction as in [26]. Extracted samples were analyzed by a liquid chromatography–tandem mass spectrometry system (QTRAP 5500; AB Sciex) equipped with an LC-20AD HPLC (Shimadzu, Tokyo, Japan). A Poroshell 120 EC-18 column (100 mm × 4.6 mm × 2.7 μm; Agilent Technologies, Santa Clara, CA) was kept in a column oven maintained at 50°C, and LM were eluted with a gradient of methanol/water/acetic acid from 55:45:0.01 (v/v/v) to 100:0:0.01 at 0.5 ml/min flow rate. To quantify the levels of targeted LM, a multiple reaction monitoring (MRM) method was devised with signature ion fragments for each molecule. Identification was conducted using published criteria including retention times and at least six signature and diagnostic ion. Calibration curves were obtained using synthetic and authentic LM mixtures, including but not limited to d_4-LTB_4, d_5-LXA_4, d_4-PGE_2, d_5-RvD2, RvD1, RvD2, RvD3, RvD4, RvD5, PD1, MaR1, RvE1, RvE2, LXA_4, LXB_4, PGE_2, PGD_2, $PGF_2\alpha$, TxB_2, and LTB_4 at 1.56, 3.12, 6.25, 12.5, 25, 50, and 100 pg. Linear calibration curves for each compound and biosynthetic pathway markers (15S-HETE, 5S-HETE, 17S-HDHA and 14S-HDHA) were obtained with r^2 values of 0.98–0.99. Quantification was carried out based on peak areas of the multiple reaction monitoring (MRM) transitions specific for each mediator using instrument settings reported in [26].

Flow Cytometry

Fresh heparinized human whole blood (100 μl) was collected from healthy volunteers under the protocol # 1999-P-001297 approved by the Partners Human Research Committee. Written informed consent was obtained from all donors. Whole blood was incubated with 10 nM of Resolvin D4, 10-trans-Resolvin D4, 10,13-trans Resolvin D4, 17-oxo-RvD4 or vehicle for 15 minutes at 37°C. *E. coli* was labeled using Baclight Green fluorescent dye according to manufacturer's protocol (Life Technologies, Grand Island, NY). Labeled *E. coli* (1:50, leukocytes to *E. coli*) was added to samples to initiate phagocytosis at 37°C for 45 minutes. Samples were then incubated with APC anti-human CD16 (neutrophils) and APC-Cy7 anti-human CD14 (monocytes) (Biolegend, San Diego, CA) for 15 minutes on ice. Cells were washed twice with 2 ml of ice-cold PBS followed by red blood cells lysis and fixed in 2% paraformaldehyde. Cells were then analyzed using BD FACS Canto II flow cytometer (BD Biosciences, Canto II). Fluorescent associated phagocytosis was measured in $CD16^+CD14^-$ neutrophils and classical monocytes $CD14^+CD16^-$ using FlowJo Version X.

Human neutrophil isolation and macrophage differentiation

Human neutrophils were isolated by density-gradient Ficoll-Histopaque from human peripheral blood. Blood was obtained from healthy human volunteers giving informed consent under protocol # 1999P001279 approved by the Partners Human Research Committee. Macrophages were prepared from peripheral blood mononuclear cells (PBMCs) purchased from Children's Hospital Blood bank. PBMCs collected from healthy donors were differentiated using GM-CSF (20 ng/mL) in RPMI culture media (Lonza) containing 10% FBS (Invitrogen), 5mM L-Glutamine (Lonza), and 5% penicillin and streptomycin

(Lonza) for 7 days. Cells were then plated in 96-well plates at 5×10^4 cells/well or 8-well chamber slides at 1×10^5 cells/well overnight before experiments.

Human Macrophage Phagocytosis

Macrophages were plated onto 96-well plates (50,000 cells/well), treated with pertussis toxin (PTX) 1 μg/ml overnight or cholera toxin (CTX) (1 μg/ml) for 2 hours at 37 °C. RvD4 (1 nM) or vehicle was incubated with cells for 15 min at 37 °C, followed by addition of BacLight Green-labeled *E. coli* (2.5×10^6 CFU) for 60 min at 37 °C. Plates were gently washed, extracellular fluorescence quenched by trypan blue, and phagocytosis determined by measuring total fluorescence (Ex 493/Em535 nm) using a fluorescent plate reader (Molecular Probes). For real-time imaging, MΦ were plated onto 8-well glass chamber slides (100,000 cells/well) and kept in a Stage Top Incubation system for microscopes equipped with a built-in digital gas mixer and temperature regulator (TOKAI HIT model INUF-K14). RvD4 or 17-oxo-RvD4 was added to the cells (10 nM; 15 min at 37°C) followed by BacLight Green-labeled *E. coli* (5×10^6 CFU). Images were then acquired every 10 min for 2h (37°C) with Keyence BZ-9000 (BIOREVO) inverted fluorescence phase-contrast microscope (40x objective) equipped with a monochrome/color switching camera using BZ-II Viewer software (Keyence, Itasca, IL, USA). Green fluorescence intensity was quantified using BZ-II Analyzer.

Real-time neutrophil chemotaxis

Human neutrophils were isolated from peripheral whole blood collected from healthy volunteers using a Ficoll-Histopaque density gradient. Red blood cells were lysed with hypotonic buffer and isolated neutrophils were resuspended in Hank's Balanced Salt Solution (HBSS, Gibco life technologies™). Neutrophils (3×10^6 cells/mL) were placed on Ibidi chemotaxis chambers following manufacturer's protocol and as described earlier [27] (μ-Slide Chemotaxis 80326, Ibidi cells in focus, Germany). Chemotaxis toward gradient of LTB_4, RvD1, RvD2, RvD3, RvD4, RvD5, 17-oxo-RvD4, 10-trans-RvD4, or 10,13-trans-RvD4 (10 nM each) or vehicle (HBSS containing 0.1% ethanol) was then recorded for a 30-minute period with a digital monochrome/color switching camera using BZ-II Viewer software (Keyence). Cell migration was analyzed using the cell-tracking function in ImageJ software. At least 60 cells per condition were analyzed from each donor for four separate donors.

Incubations of RvD4 and recombinant enzyme

Enzymatic conversion of RvD4 (1μg) was carried out by suspending RvD4 in Tris-HCL buffer (pH 9.0). Next, ~10 mM of NAD^+ (Sigma) was added followed by addition of eicosanoid oxidoreductase (EOR), i.e. 15-hydroxy prostaglandin dehydrogenase (human recombinant, 5μg, Cayman Chemicals) and incubated at 37 ºC for 2 hr [28]. The reaction mixtures were stopped with cold methanol (30–60 min), followed by centrifugation, extraction and subject to LC-MS-MS.

Statistics

Statistical analysis was performed using nonparametric tests including Student's *t* test for two-group comparisons and one-way analysis of variance (ANOVA) for multiple group comparisons with post-hoc analysis using Tukey's or ANOVA with Bonferroni Multiple Comparison Test (more than two groups) using Prism version 6 (GraphPad, La Jolla, CA USA). $P < 0.05$ was considered significant.

Results

A new total organic synthesis of RvD4

Given the pico- to nanomolar potency of resolvins [1, 4], to obtain commercial quantities of RvD4 (Fig. 1) and related isomers for further *in vivo* and *in vitro* studies, a multi-milligram total organic synthesis was carried out first by building the C1-C9 fragment in nine steps from D-ribose (Fig. 1A). The acetonide diol was deprotected, resulting in a mix of δ-lactone and hydroxyl ester. Attempts to fully open lactone **11** back to **10** (Fig. 2) were unsuccessful (Supplemental Figure 1A) so the synthesis was carried forward as a mixture. Wittig salt **14** was prepared in 2 steps [29] (Supplemental Fig. 1B). Enal **22** was prepared in seven steps (Supplemental Fig. 1C) [30, 31]. Compound **14** and **22** were coupled followed by silyl ether deprotection with TBAF affording compound **24** (Supplemental Figure 1D). Next, 50 mg of compounds **10/11** and 10 mg of $Pd[PPh_3]_4$ were dissolved in 1 ml of benzene. After stirring for 1 hr, 50 mg of **24** in 0.8 ml benzene followed by 25 μl BuNH2 and 3.2mg CuI were added. After 12 hours, reactions were stopped, extracted and isolated (see Methods).

The extent of the bioactions of RvD4 during inflammation and resolution hinges on the local biosynthesis and regulation. Enzymatic conversion of RvD4 by the eicosanoid oxidoreductase enzyme (EOR), also known as 15-hydroxy prostaglandin dehydrogenase [14], to the 17-oxo-RvD4 further metabolite is critical in the regulation of this mediator's actions (**Fig. 1B)** and was evaluated (*vide infra*). Putting this RvD4 pathway into context of how SPMs are regulated locally in tissues was critical in appreciating the actions of RvD4 in host protection and resolution *in vivo* and required quantities of synthetic RvD4 that permitted assessment of this pathway (Fig. 1B).

Next, 38.8 mg of **25/26** (Fig. 2) were recovered and carried on to the Boland reduction. Activated Zn (Cu/Ag) was prepared (380mg) and suspended in 5ml water, then 38mg of 25/26 in 5ml MeOH was added and it was stirred at 40°C for 12 hours. The reaction was diluted in MeOH and filtered over celite. Concentration to 6 ml followed by treatment with 0.5 M K_2CO_3 yielded crude RvD4 (**29**) (Supplemental Fig. 1E). RvD4 was purified by HPLC (Gemini C18, C18, 5mm, 250 × 4.6 mm), giving a λ_{max} 270 nm, MeOH/H_2O (0.1% AcOH) 75/25 v/v, 1 ml/min, T_R = 13.06 min. Structural confirmation was obtained by 1D ^1H NMR and proton coupling constants ($^nJ_{H,H}$) to provide evidence for the crucial *cis trans* assignment characteristic in the RvD4 [23] original structure elucidation from resolving exudates and human leukocytes (Supplemental Fig. 2).

Human bone marrow RvD4: matching and endogenous production

To determine whether RvD4 is present in human tissue, we carried out metabolomics profiling on healthy human bone marrow and found biologically active amounts of RvD4 (1.0 ± 0.3 pg/mL, ~2.7 pM; *vide infra*) by matching physical characteristics, namely retention profile and MS-MS diagnostic ions of synthetic to endogenous material in human bone marrow (Fig. 3). Characteristic UV absorbance of RvD4 with a λ_{max} at 276 nm and triplet band of absorbance in ethanol with shoulders at 266 nm and 285 nm also gave a broad shoulder at 233–235 nm confirmed the conjugated diene along with the conjugated triene configuration of the RvD4 backbone (Fig. 3B) [cf. ref. 24]. Targeted LC-MS-MS profiling of extracts from human bone marrow tissue matched retention time and parent/daughter mass ion directly compared to those of synthetic RvD4. Further and absolute confirmation was obtained by matching M-H=375 and at least 6 characteristic daughter ions including, m/z - 357, 339, 331, 313, 295, 255, 241, 225, 215, 113, and 101 (**Fig. 3D inset**), which clearly demonstrated that RvD4 was present in human bone marrow.

Endogenous RvD4 is produced in mouse bone marrow in response to ischemic injury

To investigate RvD4 production in response to acute sterile injury, mice underwent hind limb ischemia (HLI) by permanent femoral artery ligation and the production of RvD4 was monitored by targeted LC-MS-MS (Fig. 4). This analysis revealed that RvD4 was present in mouse bone marrow and statistically significantly increased 1 day after HLI (455 ± 170 pg/femur and tibia), compared with sham-operated animals (12.4 ± 3.5 pg) (Fig. 4A). The levels of RvD4 sharply declined by 5 days post-HLI (9.7 ± 1.8 pg), demonstrating a temporal regulation of RvD4. A representative MS-MS spectrum of RvD4 from mouse bone marrow is shown in Fig. 4B, with diagnostic ions used for identification. In addition to RvD4, we also identified its biosynthetic partner [23], namely RvD3 (16.8 ± 4.7 pg/femur and tibia). Like RvD4, RvD3 was present in bone marrow of sham-operated mice and increased in a temporal manner during HLI (Fig. 4C). We noted that levels of RvD4 at day 1 post HLI were more than 28-fold greater than that of RvD3.

RvD4 protective actions in second organ lung injury

Since RvD4 was increased with local tissue ischemia in bone (Fig. 4), we next tested RvD4 in ischemia reperfusion (reflow) injury of the lung in mice. With enough RvD4 from the commercial scale synthesis to carry out *in vivo* studies (Figs. 1 and 2), we assessed the impact of RvD4 in second organ ischemic reperfusion injury using pharmacological doses in this model of leukocyte-mediated tissue injury (Fig. 5). This is a separate *in vivo* mouse model of ischemic followed by second organ, also known as remote organ injury, where vaso-occlusion of the limb activates leukocytes locally. Next, when the vaso-occlusion is released by removing the tourniquet, neutrophils perfuse the lung and evoke collateral tissue damage [9, 20]. This system models the lung injury obtain in limb surgery. In these experiments, RvD4 was administered intravenously 50 minutes post ischemia and 10 minutes before reperfusion injury (Fig. 5A). Mice were euthanized two hours after reperfusion, and second organ reperfusion lung injury was assessed by myeloperoxidase (MPO) to determine PMN infiltration. RvD4 (500 ng/mouse, iv) reduced lung PMN infiltration with MPO levels by ~50% when directly compared to values obtained from

control lungs with ischemic reperfusion alone (Fig. 5B). RvD4 was also directly compared to the protective actions of RvD3, which was found earlier to be organ protective and pro-resolving [21, 32]. Histology samples of the second organ lung injury showed reduced infiltration of neutrophils into the lung by both RvD4 (not shown) and its comparator RvD3 and biosynthetic counterpart. Next, using state-of-the-art mass spectrometry- (MS) based metabololipidomics, lipid mediators (LM) were identified using multiple reaction monitoring via direct comparison with synthetic and authentic standards. Administration of RvD4 statistically significantly reduced the levels of pro-inflammatory eicosanoids: LTB_4 (60%), thromboxane (60%), prostaglandin E_2 (55%), and prostaglandin $F_{2\alpha}$ (52%) in the lungs of mice compared to untreated I/R mice (Fig. 5C-D). This statistically significant reduction in pro-inflammatory mediators demonstrated the potent protective actions of RvD4 in reducing second organ injury, a form of sterile acute inflammation in vivo that exemplifies leukocyte-mediated collateral tissue damage.

RvD4 structure function relationship with synthetic isomers in human whole blood

To assess the stereoselectivity of RvD4 actions, we prepared structurally related isomers. To obtain synthetic double-bond isomers of RvD4 for biological evaluation, 1 mg of RvD4 was treated with 1M LiOH in 4 ml of DME until the pH was 9–10 (see Supplement for details). Next, 0.04 mg of glutathione (mg/ml in water) was added and the reactions were monitored by HPLC [33]. The 10-trans-RvD4 (10*E*-RvD4) eluted first with T_R = 16.78 minutes followed closely by the 10,13-trans-RvD4 isomer that eluted at T_R = 17.67 min. The RvD4 starting material was essentially completely converted, as the RvD4 peak was not observed at T_R = 18.45 min via LC-MS-MS. To quench the reaction the pH was adjusted back to pH = 9 when necessary. After 26 hr the pH was adjusted to pH 5 using 3.5M AcOH. The product was purified by HPLC to afford ~0.1 mg of 10*E*-RvD4 (**Fig. 6A)**, which gave a UV absorbance with λ_{max}^{MeOH} 262, 272, 281 nm and a band shoulder at 235 nm, and 0.05 mg of 10*E*,13*E*-RvD4 (Fig. 6A), λ_{max}^{MeOH} 262, 272, 281 nm with a shoulder at 232 nm (Supplemental Fig. 3). These isomers (Fig. 6A) now permitted the assessment of the role of the double bond geometry (indicated by arrows in Fig. 6A). The 10E-isomer of RvD4 is a natural isomer formed in biosynthesis of RvD4 and by isomerization during workup [23]. The 10*E*,13*E*-RvD4 isomer is thought to be a rogue molecule used here to assess the contribution of the 13,14-double bond in the *cis* configuration in native RvD4.

Since RvD4 gave protective actions in leukocyte-mediated second organ injuries of the lung (Fig. 5), we next investigated the actions in key host defense mechanisms and resolution, namely human leukocyte phagocytosis by RvD4 and its isomers to explore structure function activity. In peripheral blood leukocyte phagocytosis, native RvD4 (4*S*,5*R*,17*S*-trihydroxydocosa-6*E*,8*E*,10*Z*,13*Z*,15*E*,19*Z* hexaenoic acid) increased *E. coli* phagocytosis greater than 50 % in $CD16^+$ (neutrophils) as well as $CD14^+$ (monocytes) compared to phagocytosis in the vehicle control as monitored by flow cytometry (Figure 10C). Enhancing phagocytosis of bacteria is a key action of resolvins and other pro-resolving mediators that promote killing and clearance [34]. More importantly, the 10*E*-RvD4 (10-trans-RvD4; 4*S*, 5*R*,17*S*-trihydroxydocosa-6*E*,8*E*,10*E*,13*Z*,15*E*,19*Z*-hexaenoic acid), a natural isomer of RvD4 produced on its biosynthesis [23], and 10*E*,13*E*-RvD4 (10,13-trans-RvD4; 4*S*,5*R*, 17*S*-trihydroxydocosa-6*E*,8*E*,10*E*,13*E*,15*E*,19*Z*-hexaenoic acid), an unnatural isomer, did

not significantly increase *E. coli* phagocytosis by peripheral blood phagocytes above that of vehicle alone (Fig. 6A-D). These results demonstrate the critical role of the specific double bond geometry and stereochemistry of RvD4 (Fig. 6A; highlighted in yellow) required for biological processes, namely neutrophil and monocyte phagocytosis of *E. coli* in human peripheral blood. Also of note, the actions of RvD4 in phagocytosis with human leukocytes proved to be cholera-toxin (CTX)-sensitive and not pertussis toxin (PTX)-sensitive (Fig. 7), suggesting a role for G_s protein and G protein-coupled receptors in RvD4-mediated actions.

Enzymatic conversion of RvD4 by eicosanoid oxidoreductase (EOR) and human bone marrow

Resolvins can undergo local inactivation *via* further metabolism [15]. We next assessed the impact of metabolic conversion via EOR to understand its role and structure of products in metabolism of RvD4. Incubating RvD4 in the presence of NAD+ (10 mM) at 37°C with EOR (0.5μg) produced 17-oxo-RvD4 (Fig. 8A). The structure of 17-oxo-RvD4 and percent conversion by EOR (>99%) were determined using reverse phase HPLC analysis and targeted LC-MS-MS. We found that the 17-oxo-RvD4 (R_T = 11.88) had an earlier retention time to that of RvD4 (R_T = 12.30) (Fig. 8B,D) and were isolated. Monitoring 17-oxo-RvD4 with LC-MS-MS at m/z 373 => 101 yielded six diagnostic daughter ions, including m/z 241 that further confirmed the conversion to the 17-oxo-containing further metabolite and structure of 17-oxo-RvD4 (Fig. 8C,E).

With this new information on the physical properties and formation of 17-oxo-RvD4, we next determined if RvD4 further metabolites are present in human tissue. Results in Figure 9 document that human bone marrow leukocytes, when incubated with RvD4, produced two further products, namely 17-oxo-RvD4 and 15,16-dihydro-RvD4, that were identified by their MS-MS and ion fragments (**Fig. 9 insets**).

Chemotaxis and phagocytosis with human leukocytes: comparisons of RvD4 and related structures

Given that 17-oxo-RvD4 is produced in human tissue, we next determined its actions compared to RvD4 (Fig. 10). Directly compared to LTB_4, none of the D-series resolvins stimulated neutrophil chemotaxis (Fig. 10A). These results are consistent with those reported earlier using different microfluidic chambers with human PMN exposed to RvD1 and RvD2 [27], which do not stimulate PMN chemotaxis. With LTB_4 as chemoattractant and positive control in a second series of experiments (Fig. 10B), we assessed whether RvD4 or the related isomer structures evoked chemotaxis. The endogenous RvD4 further metabolite 17-oxo-RvD4 had essentially no activity, nor did the two synthetic trans double-bond isomers, 10-trans-RvD4 and 10,13-trans-RvD4. Hence, the direct comparisons of 17-oxo-RvD4, 10-trans-RvD4 and 10,13-trans-RvD4 to LTB_4 in the gradient microfluidic chambers indicated that they do not on their own stimulate chemotaxis of human neutrophils (Fig. 10B).

Since RvD4 stimulates phagocytosis [24], we directly compared the 17-oxo-RvD4 to RvD4 in leukocyte phagocytosis (neutrophils and monocytes) of *E coli* in human peripheral blood and with human macrophages using real-time imaging (Fig. 10C, D). In both settings, 17-

oxo-RvD4, the further metabolite, was essentially inactive in stimulating phagocytosis compared to native RvD4, which statistically significantly enhanced phagocytosis of *E. coli* by neutrophils (~62%), monocytes (~147%) and macrophages (~40%). These results provided evidence that RvD4 enzymatic conversion to 17-oxo-RvD4 is a resolvin inactivation pathway for human leukocytes.

Discussion

In the present report, we document a new total organic synthesis of RvD4 utilizing different initial synthon building blocks enabling stereo-control (Figs. 1, 2 and Supplemental Figs. 1-2) that provided enough material at commercial scale to assess and compare biological actions both *in vivo* and *in vitro* with human and mouse cells and tissues. Separate and independent total organic synthesis of proposed biologically active novel structures are critical for confirmation of physiologic actions of a given molecule such as resolvin D4 as well as validating and confirming its proposed structure. With this new synthesis of RvD4 in hand, we report herein the first results to identify RvD4 in both human and mouse bone marrow as well as examine RvD4's regulation via EOR-dependent metabolism at the carbon-17 position of RvD4 that was also identified with human bone marrow leukocytes. The presence and matching of endogenous RvD4 with complete stereochemistry in samples obtained from both human and mouse at biologically active concentrations (0.01 – 10 nM) suggests a potential role for RvD4 in evolutionary conservation of structure-function across species.

RvD4 demonstrated organ (i.e. lung) protective actions *in vivo* during second organ remote injury of the lung in response to ischemia-reperfusion of the tissue. Also, RvD4 reduced several of the classic pro-inflammatory eicosanoids including LTB_4, TxB_2, PGE_2 and $PGF_{2\alpha}$ in this tissue. Two isomers of RvD4 were synthesized to determine structure activity relationships, namely contributions of double bonds in RvD4 and its naturally occurring biosynthetic geometric isomers [23, 35]. In human whole blood RvD4 enhanced *E. coli* phagocytosis, a pro-resolving response by both CD14+ classical-monocytes and CD16+ neutrophils by greater than 50%. This increase in phagocytic capability with RvD4 [10 nM] was not obtained with either 10-trans-RvD4 (the natural isomer of RvD4) or the 10,13-trans-RvD4 thought to be a rogue isomer tested at equimolar concentrations. This regio-specificity of RvD4 orchestrating a clear biological response not upheld by geometric isomers indicates the importance in stereochemical configuration of double bonds in the biological actions of RvD4. Earlier results indicate that RvD4 stimulates resolution of *S. aureus* infections in mice, shortening the resolution interval from $R_i = 6$ hours to $R_i = 3$ hours, as well as reducing PMN infiltration [24]. A key response of resolution that distinguishes it from anti-inflammation is the process of efferocytosis of apoptotic PMN by macrophages [4]. Specialized pro-resolving mediators (SPM) by definition limit PMN further infiltration (e.g. cessation of PMN infiltration [1]), which is required during resolution of inflammation and infections, as well as activate macrophage phagocytosis of microbes as well as efferocytosis [36]. These pro-resolving actions are fulfilled by RvD4 [24] and demonstrated herein to be stereochemically selective actions with human leukocytes.

Biological regulation of many of the SPMs is controlled by site specific further conversion by local eicosanoid oxidoreductases (EORs) that act to inactivate SPMs as well as the classical eicosanoids [14]. The EOR [14] in the present experiments catalyzed the conversion of RvD4 to a novel 17-oxo-RvD4, a further metabolite that was also identified in human bone marrow cells. Transformation of RvD4 to 17-oxo-RvD4 appears to represent the main metabolic route (Fig. 9) in blood cells and bone marrow. In comparison, RvD1 is also rapidly metabolized by recombinant EOR/15-PGDH, reaching maximal conversion within 20 min as measured by NADH levels [28]. It is likely that EOR conversion of RvD4 shares similar kinetics. Along these lines, it is noted in the present study that in mouse bone marrows following ischemic injury, RvD4 levels were the highest at Day 1 (455±170 pg/ femur and tibia), followed by a decline at Days 5–10 (Fig. 4). It is possible that bone marrow leukocytes contain EOR that rapidly metabolized RvD4, contributing to the sharply reduced levels of RvD4 in Days 5 and 10. In comparison, in the ischemia-initiated second organ injury, RvD4 levels were 51.3±18.5 pg/100 mg lung tissue 2h following reperfusion (n=4). Since EOR/15-PGDH is highly expressed in lungs [28], it is likely that RvD4 was also rapidly converted by EOR in lungs. It remains of interest to determine whether RvD3 is a substrate for EOR.

We found 17-oxo-RvD4 inactive at enhancing phagocytosis of *E. coli* by human neutrophils, monocytes and macrophages compared to its metabolic precursor RvD4 (Fig. 10). These findings were similar to those with RvD1: as documented earlier, 17-oxo-RvD1 is the primary inactivation site, while the related 8-oxo-RvD1 metabolite remained active [28]. For comparison, another resolvin, RvD2, is converted to both 7-oxo-RvD2 and 16-oxo-RvD2 in adipose tissues, with 7-oxo-RvD2 being the major metabolic route that remains active on adipose-directed actions, whereas 16-oxo-RvD2 proves inactive [37]. A limitation of the present experiments is that future studies are needed to interrogate fully the biological relevance of this newly identified metabolic route of RvD4 conversion to the 17-oxo-containing metabolite and its potential inactivation in other human cell types and tissues. Our main goal in these experiments was to address and further establish the complete structure of RvD4 [23, 24], its scale-up synthesis and the confirmation and rigorous validation of stereochemical selectivity in RvD4 functional responses. Also, these results provide evidence for a likely G protein coupled receptor(s) that evokes intracellular signaling in response to RvD4, the identity of which remains to be determined.

In summation, the present findings reported herein demonstrate a new larger-scale total organic synthesis of RvD4 as well as document the pro-resolving and organ-protective actions of RvD4 in second-organ reflow injury of the lung. We also identified endogenous production of RvD4 in both human and mouse bone marrow that was increased following ischemia. In addition, RvD4's structure-function activity was determined for the regulation of leukocyte responses. The 17-oxo-RvD4 novel further metabolite of RvD4 identified with human bone marrow cells and the trans double-bond-containing isomers of RvD4 showed diminished or no apparent biological activities compared to the native RvD4 stereochemistry. These results emphasize the importance of stereoselectivity in the activation of pro-resolving leukocyte responses with RvD4, and provided structural basis to develop longer acting analogs that resist enzymatic inactivation [15]. Importantly, the availability of commercial quantities of rigorously validated RvD4 as reported herein as well as other

SPMs will help promote the advancement of resolution-phase agonists as potential new approaches for controlling pathologies linked to excessive neutrophil-mediated collateral tissue damage and organ injury, excessive inflammation, as well as interrogating failed resolution mechanisms in cellular and in vivo systems.

Supplementary Material

Refer to Web version on PubMed Central for supplementary material.

Acknowledgements/grant support

The authors thank Mary Halm Small for expert assistance in manuscript preparation. In addition, we thank Chad Araneo (Harvard University) for assistant with flow cytometry, Ian Riley, Justin English and Molly Jenssen (Center for Experimental Therapeutics and Reperfusion Injury, Brigham & Women's Hospital) for technical assistance and cell isolations. This study was supported by National Institutes of Health grant P01GM095467.

Abbreviations

4-HDHA	4-hydroxy-docosahexaenoic acid
10E Resolvin D4	4*S*,5*R*,17*S*-trihydroxydocosa- 6*E*,8*E*,10*E*,13*Z*,15*E*-hexaenoic acid
10E,13E Resolvin D4	4*S*,5*R*,17*S*-trihydroxydocosa −6*E*,8*E*,10*E*,13*E*,15*E*-hexaenoic acid
ALX	lipoxin A_4 receptor
DHA	docosahexaenoic acid
EOR	eicosanoid oxidoreductase
HPLC	high pressure liquid chromatography
LM	lipid mediator; **MPO**, myeloperoxidase
MS-MS	tandem mass spectrometry
NMR	nuclear magnetic resonance
PMN	polymorphonuclear leukocyte
RvD1	7*S*,8*R*,17*S*-trihydroxydocosa- 4*Z*,9*E*,11*E*, 13*Z*,15*E*,19*Z*-hexaenoic acid
RvD2	7*S*,16*R*,17*S*-trihydroxydocosa- 4*Z*,8*E*,10*Z*,12*E*,14*E*, 19*Z*-hexaenoic acid
RvD3	4*S*,11*R*,17*S*-trihydroxydocosa- 5*Z*,7*E*,9*E*,13*Z*,15*E*,19*Z*-hexaenoic acid
RvD4	4*S*,5*R*,17*S*-trihydroxydocosa- 6*E*,8*E*,10*Z*,13*Z*,15*E, 19Z*-hexaenoic acid

17-oxo-RvD4	4*S*,5*R*-dihydroxy-17-oxo-6*E*,8*E*,10*Z*,13*Z*,15*E, 19Z*-docosahexaenoic acid
SPM	specialized pro-resolving mediator

References

1. Serhan CN (2014) Pro-resolving lipid mediators are leads for resolution physiology. Nature 510, 92–101. [PubMed: 24899309]
2. Vik A, Dalli J, Hansen TV (2017) Recent advances in the chemistry and biology of anti-inflammatory and specialized pro-resolving mediators biosynthesized from n-3 docosapentaenoic acid. Bioorg. Med. Chem. Lett. 27, 2259–2266. [PubMed: 28408222]
3. Cotran RS, Kumar V, Collins T (1999) Robbins Pathologic Basis of Disease. W.B. Saunders Co., Philadelphia 1425.
4. Serhan CN and Savill J (2005) Resolution of inflammation: the beginning programs the end. Nat. Immunol. 6, 1191–1197. [PubMed: 16369558]
5. Serhan CN, Brain SD, Buckley CD, Gilroy DW, Haslett C, O'Neill LAJ, Perretti M, Rossi AG, Wallace JL (2007) Resolution of inflammation: state of the art, definitions and terms. FASEB J. 21, 325–332. [PubMed: 17267386]
6. Tabas I and Glass CK (2013) Anti-inflammatory therapy in chronic disease: challenges and opportunities. Science 339, 166–72. [PubMed: 23307734]
7. Clish CB, Sun YP, Serhan CN (2001) Identification of dual cyclooxygenase-eicosanoid oxidoreductase inhibitors: NSAIDs that inhibit PG-LX reductase/LTB(4) dehydrogenase. Biochem. Biophys. Res. Commun. 288, 868–74. [PubMed: 11688989]
8. Perretti M, Cooper D, Dalli J, Norling LV (2017) Immune resolution mechanisms in inflammatory arthritis. Nat Rev Rheumatol 13, 87–99. [PubMed: 28053331]
9. Kasuga K, Yang R, Porter TF, Agrawal N, Petasis NA, Irimia D, Toner M, Serhan CN (2008) Rapid appearance of resolvin precursors in inflammatory exudates: novel mechanisms in resolution. J. Immunol. 181, 8677–8687. [PubMed: 19050288]
10. Miki Y, Yamamoto K, Taketomi Y, Sato H, Shimo K, Kobayashi T, Ishikawa Y, Ishii T, Nakanishi H, Ikeda K, Taguchi R, Kabashima K, Arita M, Arai H, Lambeau G, Bollinger JM, Hara S, Gelb MH, Murakami M (2013) Lymphoid tissue phospholipase A2 group IID resolves contact hypersensitivity by driving antiinflammatory lipid mediators. J. Exp. Med. 210, 1217–34. [PubMed: 23690440]
11. Murakami M, Taketomi Y, Miki Y, Sato H, Hirabayashi T, Yamamoto K (2011) Recent progress in phospholipase A(2) research: from cells to animals to humans. Prog. Lipid Res. 50, 152–92. [PubMed: 21185866]
12. Dinarello CA (2009) Immunological and inflammatory functions of the interleukin-1 family. Annu. Rev. Immunol. 27, 519–50. [PubMed: 19302047]
13. Levy BD, Kohli P, Gotlinger K, Haworth O, Hong S, Kazani S, Israel E, Haley KJ, Serhan CN (2007) Protectin D1 is generated in asthma and dampens airway inflammation and hyper-responsiveness. J. Immunol. 178, 496–502. [PubMed: 17182589]
14. Clish CB, Levy BD, Chiang N, Tai H-H, Serhan CN (2000) Oxidoreductases in lipoxin A_4 metabolic inactivation. J. Biol. Chem. 275, 25372–25380. [PubMed: 10837478]
15. Arita M, Oh S, Chonan T, Hong S, Elangovan S, Sun Y-P, Uddin J, Petasis NA, Serhan CN (2006) Metabolic inactivation of resolvin E1 and stabilization of its anti-inflammatory actions. J. Biol. Chem. 281, 22847–22854. [PubMed: 16757471]
16. Shireman PK (2007) The chemokine system in arteriogenesis and hind limb ischemia. J. Vasc. Surg. 45 Suppl A, A48–56. [PubMed: 17544024]
17. Zhang MJ, Sansbury BE, Hellmann J, Baker JF, Guo L, Parmer CM, Prenner JC, Conklin DJ, Bhatnagar A, Creager MA, Spite M (2016) Resolvin D2 Enhances Postischemic Revascularization While Resolving Inflammation. Circulation 134, 666–80. [PubMed: 27507404]

18. Spite M, Norling LV, Summers L, Yang R, Cooper D, Petasis NA, Flower RJ, Perretti M, Serhan CN (2009) Resolvin D2 is a potent regulator of leukocytes and controls microbial sepsis. Nature 461, 1287–1291. [PubMed: 19865173]

19. Hellingman AA, Bastiaansen AJ, de Vries MR, Seghers L, Lijkwan MA, Lowik CW, Hamming JF, Quax PH (2010) Variations in surgical procedures for hind limb ischaemia mouse models result in differences in collateral formation. Eur. J. Vasc. Endovasc. Surg. 40, 796–803. [PubMed: 20705493]

20. Qiu F-H, Wada K, Stahl GL, Serhan CN (2000) IMP and AMP deaminase in reperfusion injury down-regulates neutrophil recruitment. Proc. Natl. Acad. Sci. USA 97, 4267–4272. [PubMed: 10760293]

21. Dalli J, Winkler JW, Colas RA, Arnardottir H, Cheng CYC, Chiang N, Petasis NA, Serhan CN (2013) Resolvin D3 and aspirin-triggered resolvin D3 are potent immunoresolvents. Chem. Biol. 20, 188–201. [PubMed: 23438748]

22. Nielsen MM, Lambertsen KL, Clausen BH, Meyer M, Bhandari DR, Larsen ST, Poulsen SS, Spengler B, Janfelt C, Hansen HS (2016) Mass spectrometry imaging of biomarker lipids for phagocytosis and signalling during focal cerebral ischaemia. Sci Rep 6, 39571. [PubMed: 28004822]

23. Serhan CN, Hong S, Gronert K, Colgan SP, Devchand PR, Mirick G, Moussignac R-L (2002) Resolvins: a family of bioactive products of omega-3 fatty acid transformation circuits initiated by aspirin treatment that counter pro-inflammation signals. J. Exp. Med. 196, 1025–1037. [PubMed: 12391014]

24. Winkler JW, Orr SK, Dalli J, Cheng CY, Sanger JM, Chiang N, Petasis NA, Serhan CN (2016) Resolvin D4 stereoassignment and its novel actions in host protection and bacterial clearance. Sci Rep 6, 18972. [PubMed: 26743932]

25. Chiang N, Dalli J, Colas RA, Serhan CN (2015) Identification of resolvin D2 receptor mediating resolution of infections and organ protection. J. Exp. Med. 212, 1203–17. [PubMed: 26195725]

26. English JT, Norris PC, Hodges RR, Dartt DA, Serhan CN (2017) Identification and profiling of specialized pro-resolving mediators in human tears by lipid mediator metabolomics. Prostaglandins Leukot. Essent. Fatty Acids 117, 17–27. [PubMed: 28237084]

27. Norling LV, Headland SE, Dalli J, Arnardottir HH, Haworth O, Jones HR, Irimia D, Serhan CN, Perretti M (2016) Proresolving and cartilage-protective actions of resolvin D1 in inflammatory arthritis. JCI Insight 1, e85922. [PubMed: 27158677]

28. Sun Y-P, Oh SF, Uddin J, Yang R, Gotlinger K, Campbell E, Colgan SP, Petasis NA, Serhan CN (2007) Resolvin D1 and its aspirin-triggered 17*R* epimer: stereochemical assignments, anti-inflammatory properties and enzymatic inactivation. J. Biol. Chem. 282, 9323–34. [PubMed: 17244615]

29. Darses B, Michaelides IN, Sladojevich F, Ward JW, Rzepa PR, Dixon DJ (2012) Expedient construction of the [7–5-5] all-carbon tricyclic core of the Daphniphyllum alkaloids daphnilongeranin B and daphniyunnine D. Org Lett 14, 1684–7. [PubMed: 22404493]

30. Rodriguez AR and Spur BW (2004) First total synthesis of 7(*S*),16(*R*),17(*S*)-Resolvin D2, a potent anti-inflammatory lipid mediator. Tetrahedron Lett. 45, 8717–8720.

31. Rodriguez AR and Spur BW (2005) First total synthesis of 7(S),17(S)-resolvin D5, a potent anti-inflammatory docosanoid. Tetrahedron Lett. 46, 3623–3627.

32. Norris PC, Arnardottir H, Sanger JM, Fichtner D, Keyes GS, Serhan CN (2016) Resolvin D3 multi-level proresolving actions are host protective during infection. Prostaglandins Leukot. Essent. Fatty Acids, doi: 10.1016/j.plefa.2016.01.001.

33. Atrache V, Sok DE, Pai JK, Sih CJ (1981) Formation of 11-trans slow reacting substances. Proc. Natl. Acad. Sci. U. S. A. 78, 1523–6. [PubMed: 6112746]

34. Chiang N, Fredman G, Bäckhed F, Oh SF, Vickery TW, Schmidt BA, Serhan CN (2012) Infection regulates pro-resolving mediators that lower antibiotic requirements. Nature 484, 524–528. [PubMed: 22538616]

35. Sapieha P, Stahl A, Chen J, Seaward MR, Willett KL, Krah NM, Dennison RJ, Connor KM, Aderman CM, Liclican E, Carughi A, Perelman D, Kanaoka Y, Sangiovanni JP, Gronert K, Smith

LE (2011) 5-Lipoxygenase metabolite 4-HDHA is a mediator of the antiangiogenic effect of omega-3 polyunsaturated fatty acids. Sci Transl Med 3, 69ra12.

36. Buckley CD, Gilroy DW, Serhan CN (2014) Proresolving lipid mediators and mechanisms in the resolution of acute inflammation. Immunity 40, 315–27. [PubMed: 24656045]
37. Clària J, Dalli J, Yacoubian S, Gao F, Serhan CN (2012) Resolvin D1 and resolvin D2 govern local inflammatory tone in obese fat. J. Immunol. 189, 2597–2605. [PubMed: 22844113]

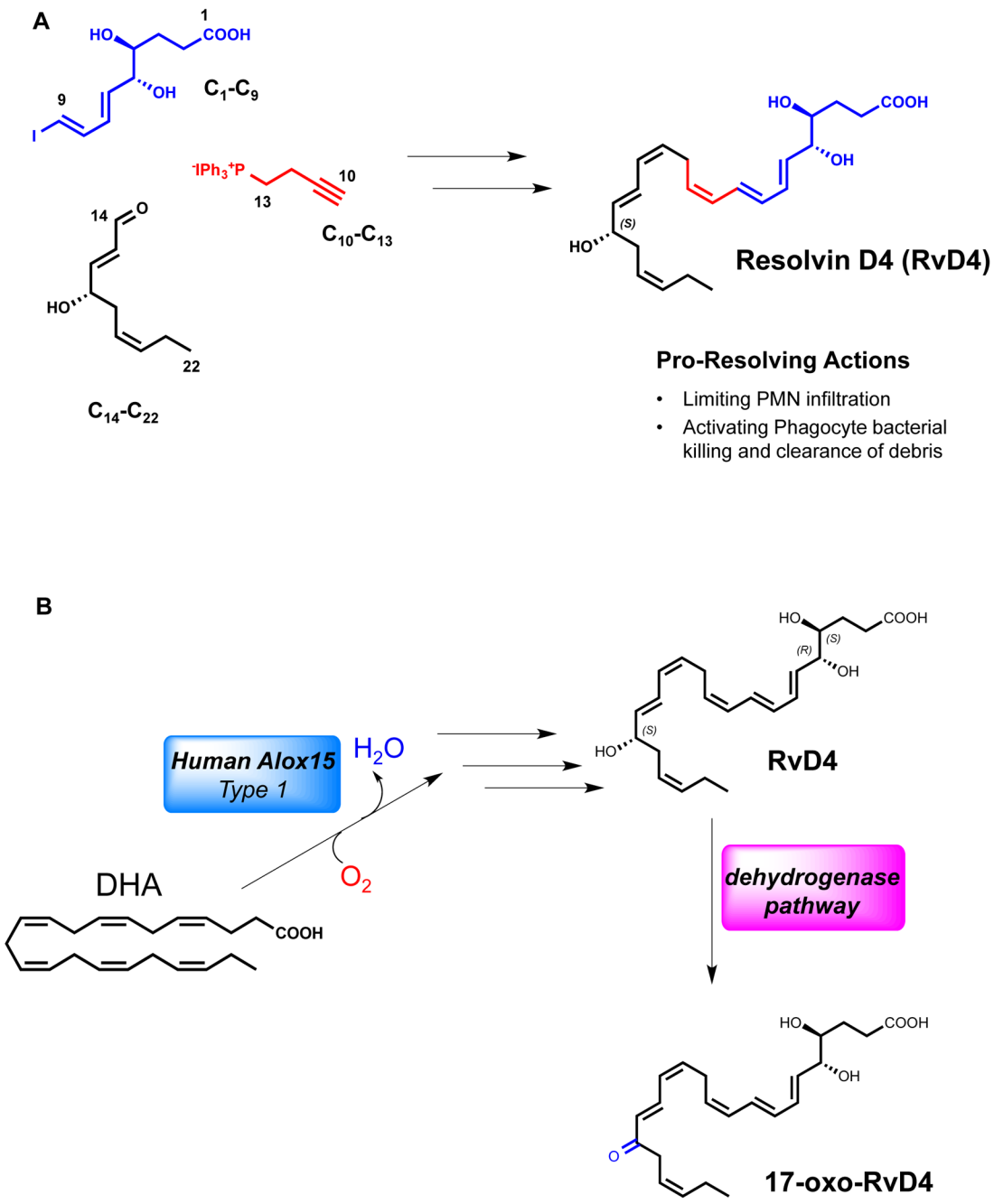

Figure 1. New retrosynthetic strategy for the total synthesis of Resolvin D4.

Stable building blocks were synthesized to afford RvD4. (A) The C1-C9 fragment was prepared in nine steps from D-ribose. C14-C22 was accomplished in seven steps and coupled by Sonogashira conditions with C10-C13, synthesized in three steps from commercially available starting material 3-Butyn-1-ol. Sonogashira coupling of precursor C10-C22 with C1-C9 followed by Boland reduction and base hydrolysis afforded RvD4. (B) The biosynthetic pathway of Resolvin D4 involves subsequent enzymatic transformations to a 4,5-epoxide intermediate in a stereo-controlled biosynthesis [23, 24] to afford the potent

pro-resolving mediator RvD4. The conversion pathway by oxidoreductase yields the 17-oxo-RvD4 further metabolite.

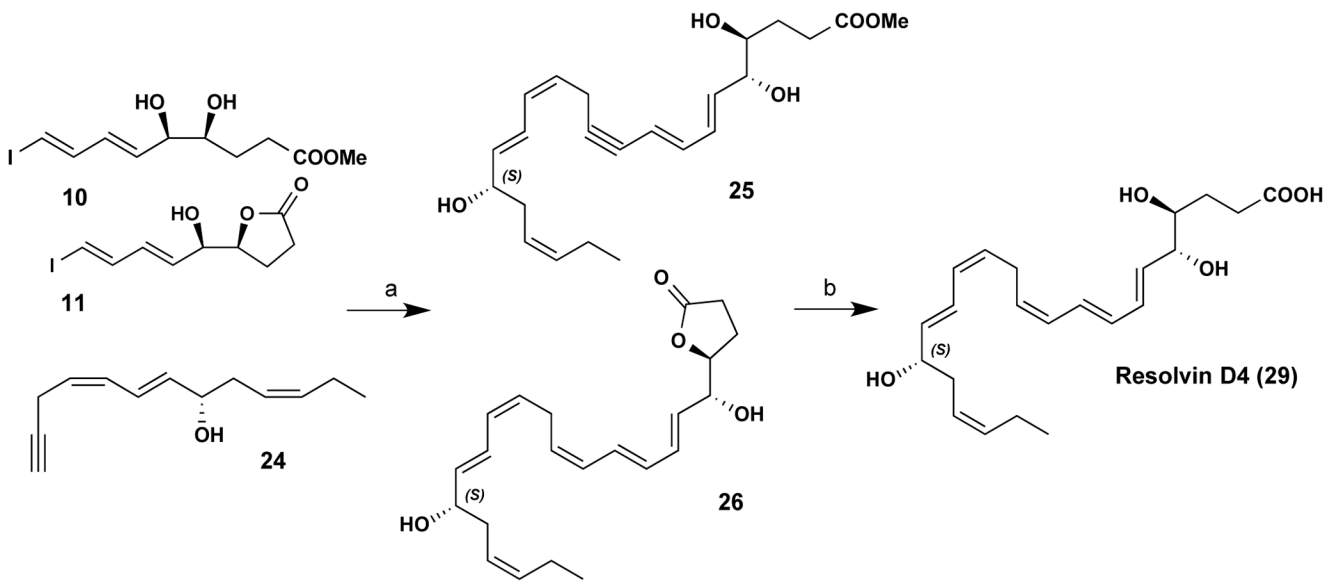

Figure 2. Critical steps in RvD4 scale-up synthesis.

See text for details on Compounds 25 and 26 to yield Compound 29.

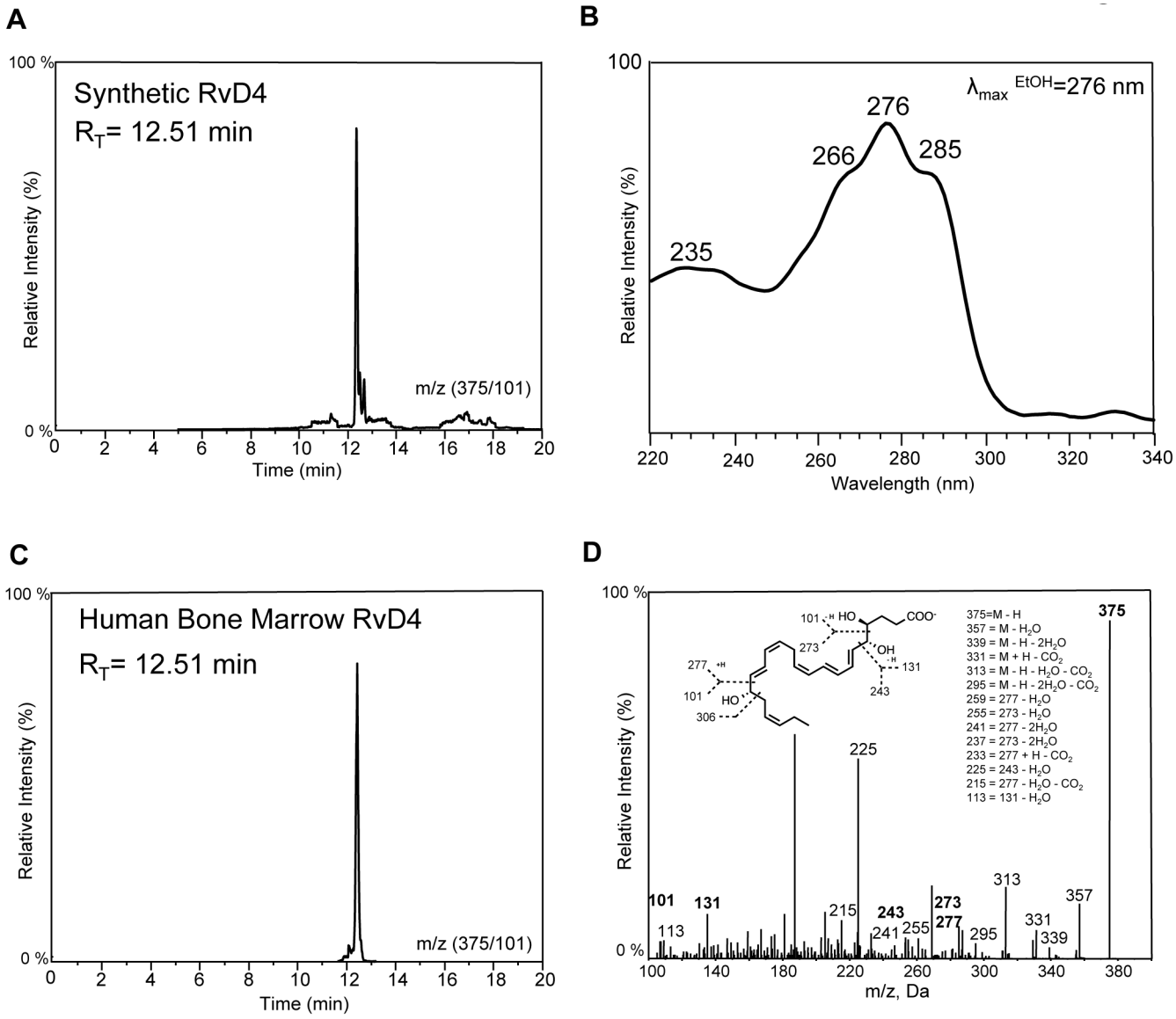

Figure 3. Matching of endogenous RvD4 in human bone marrow with synthetic material.

Synthetic material was analyzed and matched with endogenous RvD4. (A) Retention profile of synthetic material by reverse phase HPLC analysis. (B) Characteristic UV-Vis spectrum of synthetic RvD4 obtained in ethanol with a λ_{max} of 276 nm, triplet of absorbance and a shoulder of 233 nm. (C) Retention profile of endogenous RvD4 production in human bone marrow tissue. (D) LC-MS-MS of endogenous RvD4 matching synthetic material using a minimum of 6 diagnostic ions (inset) and retention time (R_T) for identification. These results are representative of n = 4.

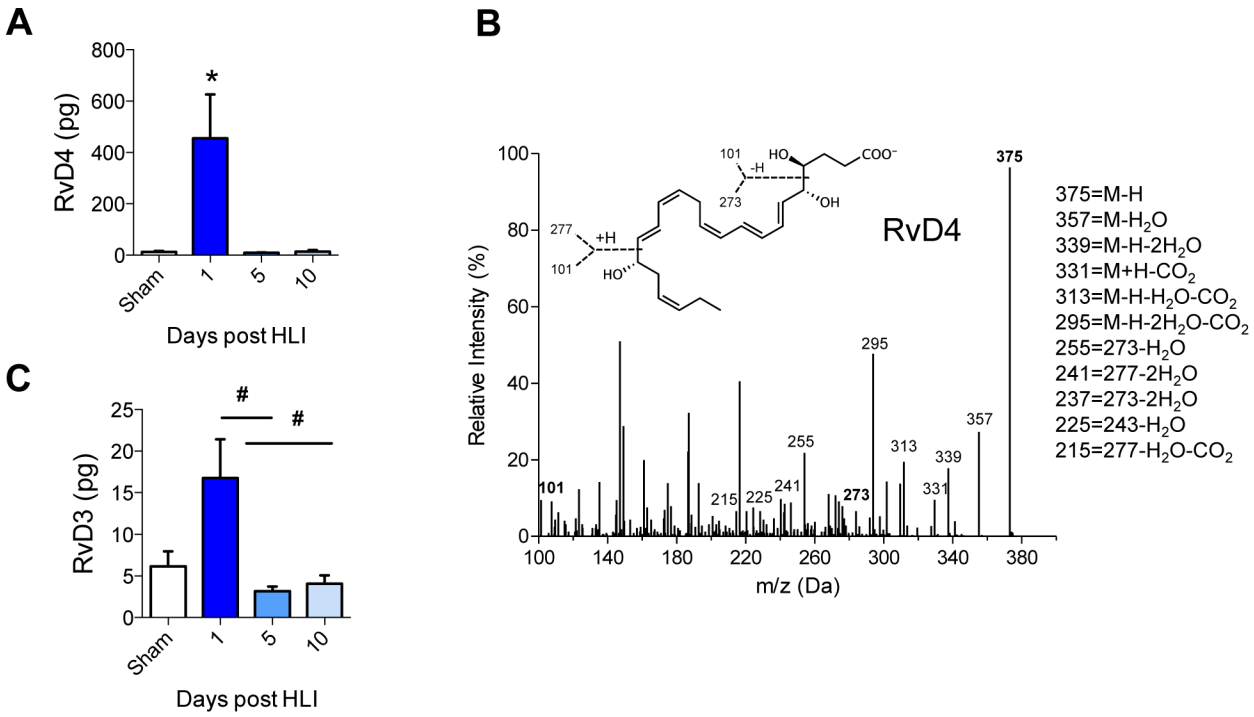

Figure 4. Permanent femoral artery ligation and production of RvD4 in local ischemic bone marrow.

Mice underwent permanent femoral artery ligation surgery and were monitored over ten days. (A) Production of RvD4 (pg/femur and tibia) over three time intervals to 10 days in bone marrow of mice undergoing hind limb ischemia (HLI) surgery, n = 3 (sham) and n =4–7 (group/time point). (B) MS-MS of RvD4 via identification of a minimum of 6 characteristic daughter ions. (C) RvD3 production during HLI. Statistical results are mean ± SEM, n=4–7, *p<0.05, vs. sham; #p<0.05 vs Day 1, one-way ANOVA.

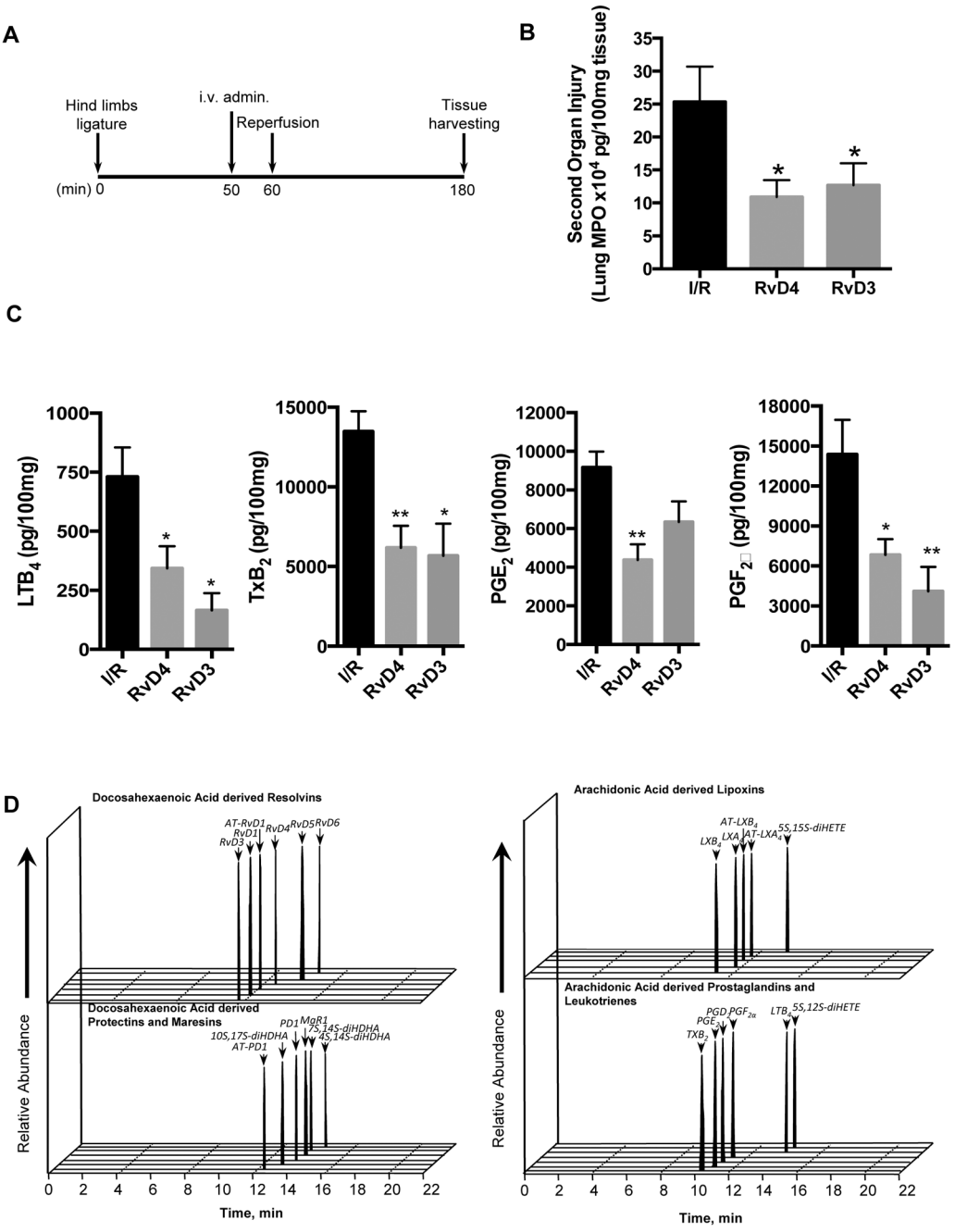

Figure 5. RvD4 displays potent organ protection *in vivo*.

Acute hind limb ischemia-reperfusion was induced by applying tourniquets to the hind limb of 6–8-week-old male C57BL6j mice. (A) Timeline: After 60 min, tourniquets were removed and reperfusion ensued for 120 min. Ten minutes prior to reperfusion, vehicle (saline containing 0.1% ethanol) and either RvD4 (500 ng) or RvD3 (500 ng) were administered i.v. Then animals were sacrificed 120 min after reperfusion. (B) Lungs were collected and MPO levels were assessed by ELISA. (C) Lungs were extracted, and resolvin, protectin, maresin, lipoxin, prostanoid and leukotriene levels were assessed by lipid mediator metabololipidomics (see Materials and Methods). Results are mean ± SEM. n=4–7.

*p<0.05, **p<0.01, vs. vehicle group. One-way ANOVA with Dunnett multiple comparison test. (D) Representative MRM chromatographs of AA, EPA and DHA bioactive metabolomes from lungs collected from vehicle group (I/R alone).

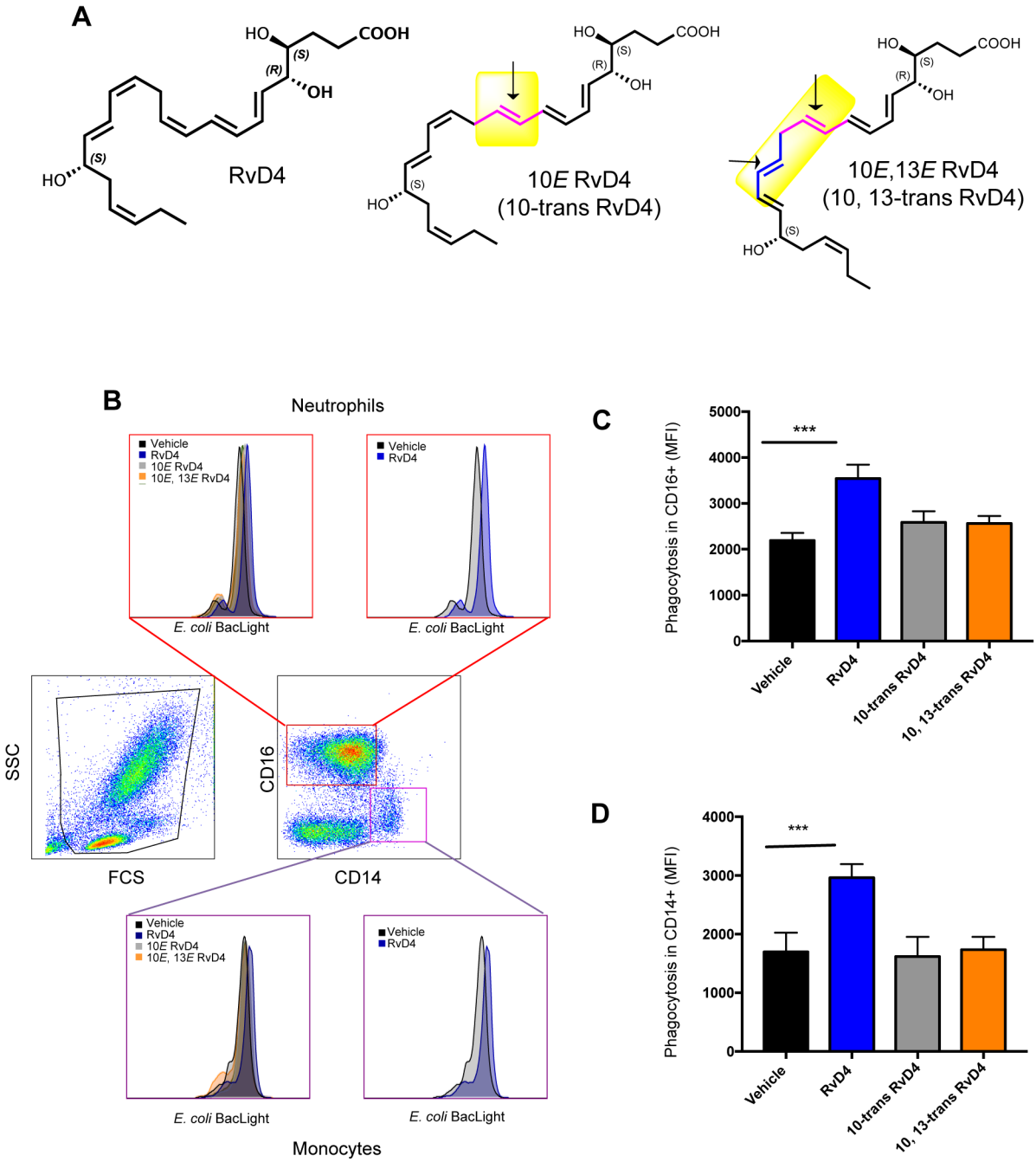

Figure 6. RvD4 increases phagocytosis in human peripheral blood neutrophils and monocytes: comparison with RvD4 geometric isomers.

(A) RvD4, 10*E*-RvD4 (10-trans-RvD4) and 10*E*,13*E*-RvD4 (10,13-trans-RvD4): Arrow indicates position of isomerized trans double bonds in these RvD4 isomers. (B-D) Fresh heparinized whole blood (100 μl) was collected from healthy donors and incubated with RvD4, 10-trans RvD4, 10,13 trans RvD4 (10 nM) or vehicle (0.1 % ethanol) for 15 minutes at 37°C followed by incubation with BacLight Green-labeled *E. coli* (1:50, leukocytes to *E. coli*). Fluorescence associated phagocytosis was monitored by flow cytometry. (B) Representative dot plots and histograms. Results are expressed as MFI representing

phagocytosis associated with (C) $CD16^+$ (neutrophils) and (D) CD14+ (monocytes) cells. Results are mean±SEM, n=3 individual donors. *** P<0.001 vs. vehicle control using one-way ANOVA with Bonferroni Multiple Comparison Test.

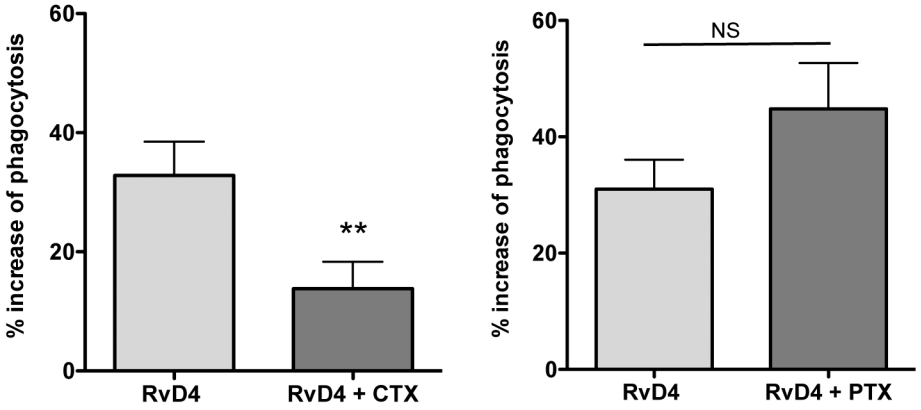

Figure 7. RvD4 stimulates phagocytosis of *E. coli* by human macrophages: toxin sensitivity.

Human macrophages were treated with pertussis toxin (PTX) or cholera toxin (CTX), each at a concentration of 1 μg/ml. RvD4 (1 nM) or vehicle was incubated with cells for 15 min at 37 °C, followed by addition of BacLight Green-labeled *E. coli* (2.5×10^6 CFU) for 60 min at 37 °C. Phagocytosis was determined using a fluorescent plate reader. Results are expressed as percent increase above vehicle control (*E. coli* alone); mean±SEM from 6 individual donors. **P<0.01, two-tailed paired t-test.

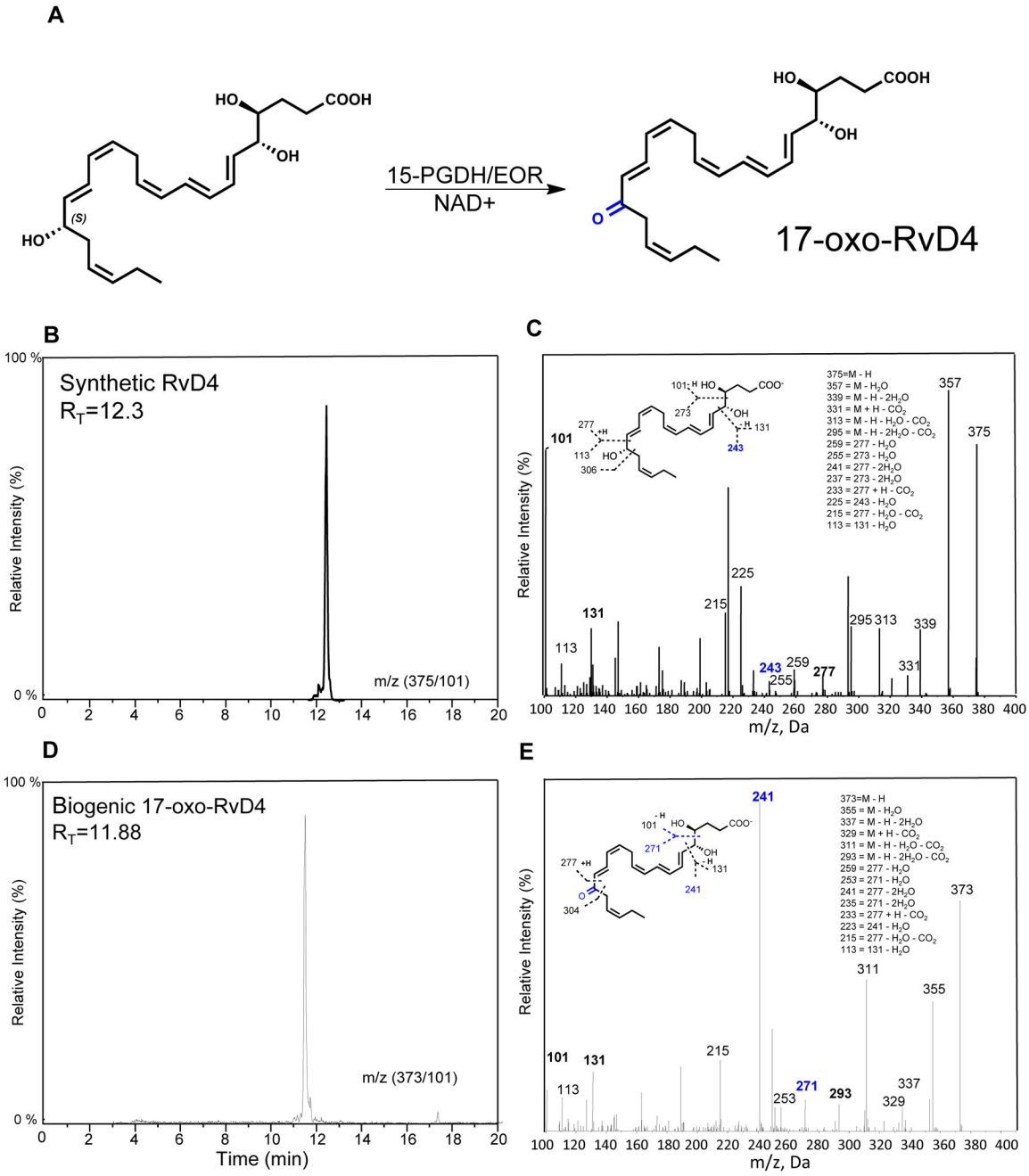

Figure 8. Enzymatic conversion of RvD4 to further metabolites.

(A) RvD4 was incubated with 15-PGDH (EOR) (10μg) at 37 °C (0.1 M Tris-HCL, pH 9.0, 10 mM NAD+, 200 μl of total volume) for 2 h. The incubations were stopped, extracted and analyzed by LC-MS-MS and HPLC. (B) Characteristic retention times of RvD4 by reverse phase LC and (C) RvD4 MS-MS. Inset: structure of RvD4 and diagnostic ions. (D) LC Retention time chromatography of 17-oxo-RvD4. (E) 17-oxo-RvD4 MS-MS. Inset: structure of 17-oxo-RvD4 and diagnostic ions.

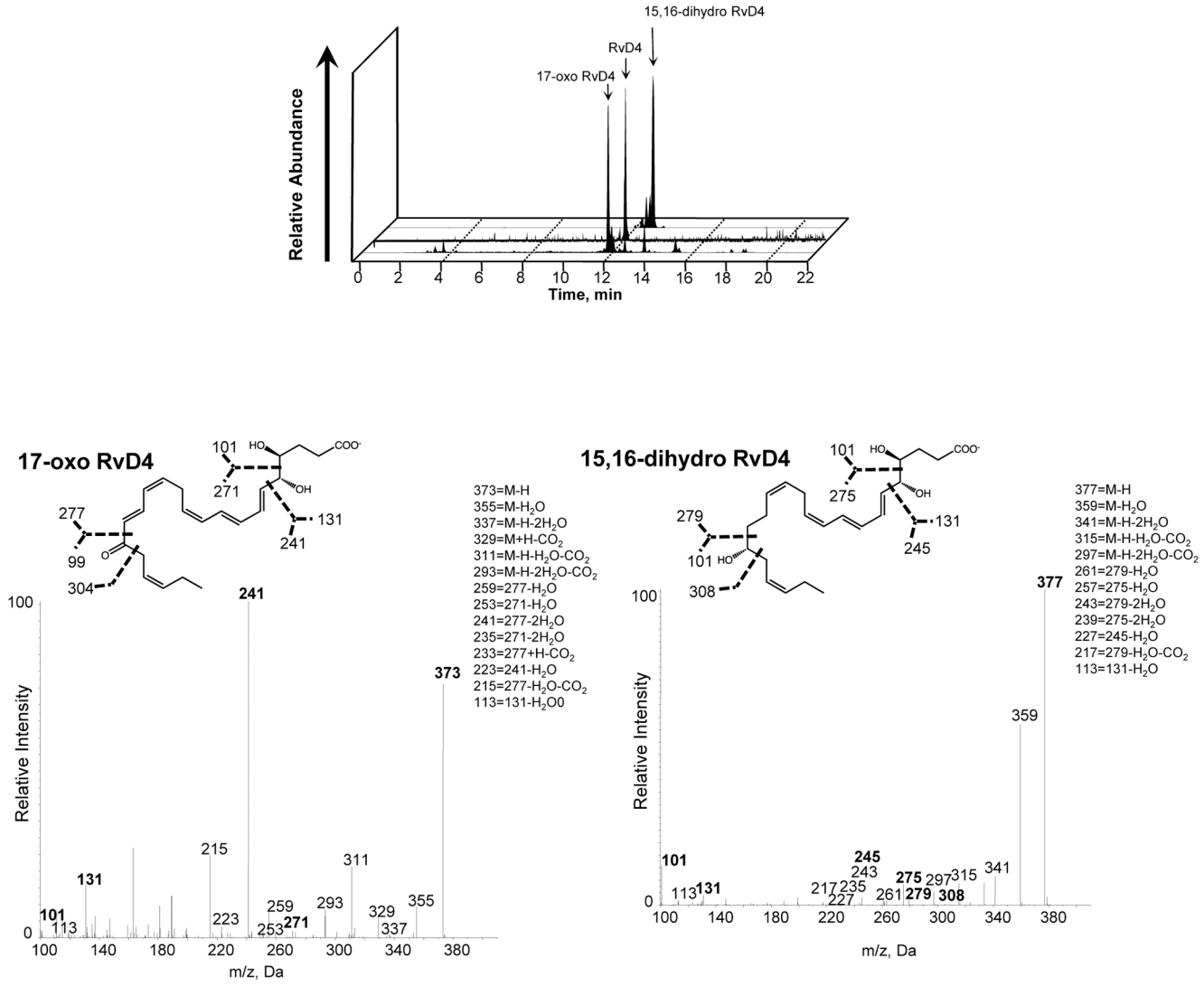

Figure 9. Human bone marrow leukocytes: Identification of RvD4 further metabolites.

Human bone marrow-derived leukocytes were isolated and incubated with RvD4 (1 μg per 100×10^6 cells/0.1 ml PBS, pH 7.45, 37°C, 120 min). Products were extracted and subject to LM-metabololipidomics (see Materials and Methods). (Upper panel) Chromatograms of RvD4 and metabolites. (Left panel) 17-oxo-RvD4 MS-MS with prominent diagnostic ions. (Right panel) 15,16-dihydro-RvD4 MS-MS with prominent ions and their assignments (inset). n=3 separate marrow donors.

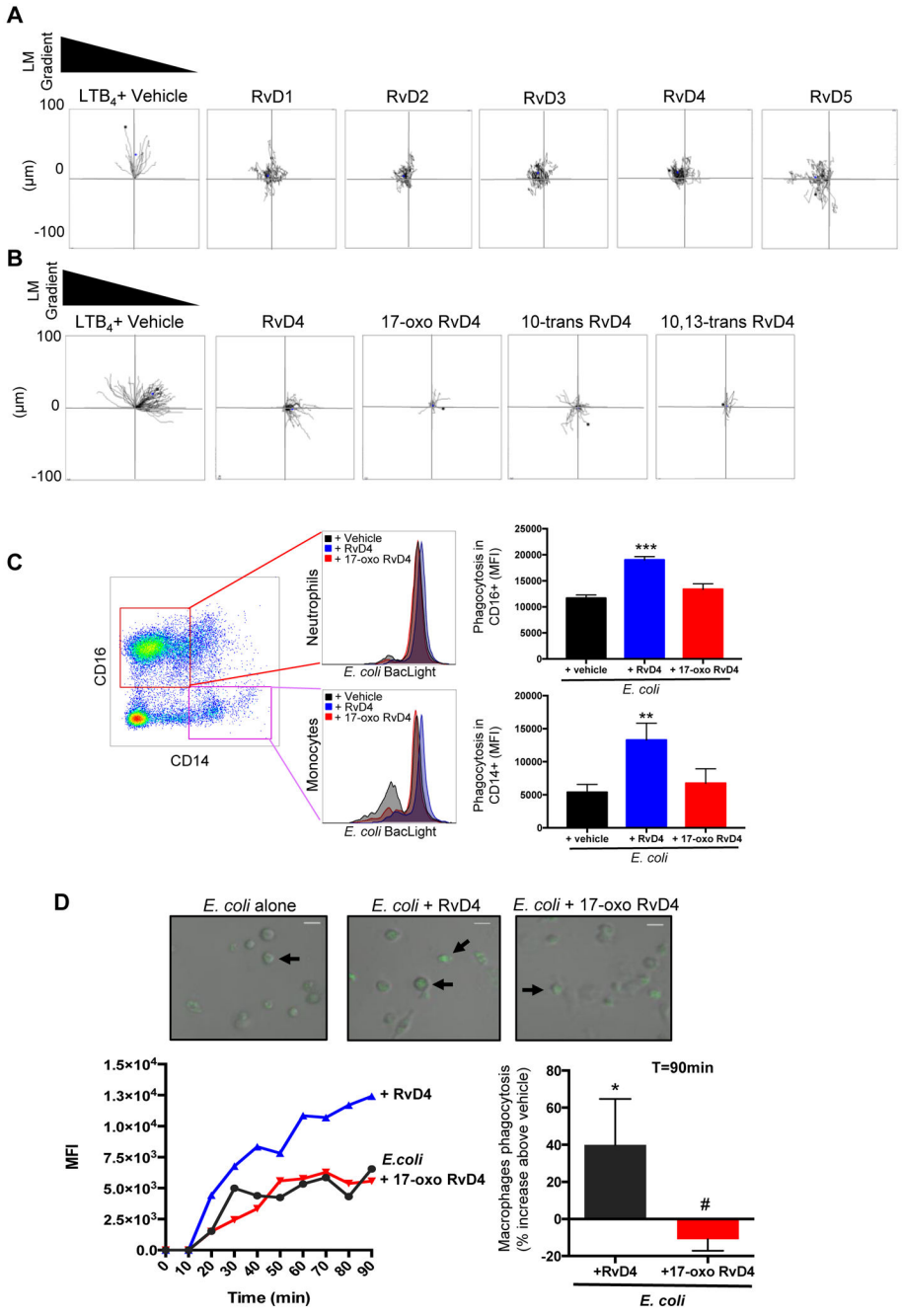

Figure 10. Human leukocyte function of RvD4

(A) Human neutrophils were isolated from peripheral whole blood (see methods). Isolated neutrophils (3×10^6 cells/ml) were placed on ibidi microfluidics chambers for chemotaxis toward RvD1, RvD2, RvD3, RvD4, RvD5 or LTB_4 (10nM each) plus vehicle (HBSS plus 0.1 % ethanol). Results are representative trajectory neutrophil paths from n=4 individual donors. B) Chemotaxis of neutrophils toward LTB_4, RvD4, 17-oxo-RvD4, 10-trans-RvD4, 10,13-trans-RvD4 (10nM each) or vehicle (HBSS plus 0.1% ethanol) was monitored in real time for 30 minutes. Representative trajectory neutrophil paths from n=4 individual donors. (C) Fresh whole blood was collected from healthy donors and incubated with either RvD4,

17-oxo RvD4 (10nM) or vehicle (0.1 % ethanol) for 15 minutes at 37°C followed by incubation with BacLight Green-labeled *E. coli* (1:50, leukocyte:*E. coli*). Fluorescence associated with CD16+ (Neutrophils) and CD14+ (monocytes) was monitored by flow cytometry. Results are mean SEM, n=3 individual donors. *** P<0.001 **P<0.01 versus *E. coli* plus vehicle using one-way ANOVA with Bonferroni Multiple Comparison Test. (D) Differentiated human monocyte derived-macrophages were plated onto chamber slides (1×10^5 cells/well). Macrophages were incubated with vehicle (containing 0.1% ethanol), RvD4, or 17-oxo RvD4 10nM for 15min at 37°C. Phagocytosis was initiated by addition of Baclight green-labeled™ *E. coli* with a 1:50 ratio (macrophages:*E. coli*), and monitored by real-time imaging. In each experiment, four fields (40x) per condition (per well) were recorded. (Top panels) Representative images: overlay of fluorescent and bright fields. Arrows indicate macrophages with ingested fluorescent *E. coli*. (Left panel) Representative time course (0–90 min) of phagocytosis. (Right) Results are expressed as percent increase of phagocytosis above *E. coli* alone at 90 min; mean±SEM, n=3. *p<0.05 *vs. E. coli* alone, $^{\#}p$<0.05 vs *E. coli* plus RvD4 using 2-tailed paired Student's *t* test.